

# Application of network pharmacology, bioinformatics, computational molecular docking, and experimental validation to study the anticancer effects of oleanolic acid in oral squamous carcinoma cells

TING YIN<sup>1</sup>   
HAO WANG<sup>2</sup>   
YAQIN ZOU<sup>2,\*</sup> 

<sup>1</sup> Department of Medicine  
Linfen Vocational and Technical  
College, Linfen City, Shanxi  
041000, China

<sup>2</sup> Department of Stomatology  
Affiliated Hospital of  
Guangdong Medical University  
Zhanjiang City, Guangdong  
Province, 524001, China

## ABSTRACT

Oleanolic acid (OA) has demonstrated anticancer effects across various cancers, with some derivatives advancing to clinical trials. However, its precise mechanisms of action remain unclear, especially in oral squamous cell carcinoma (OSCC). This study employed network pharmacology, bioinformatics, molecular docking, dynamics simulations, and experimental validation to explore OA's anticancer effects in OSCC and elucidate its mechanism of action. OA's pharmacokinetic and physicochemical properties were assessed using SwissADME and Molsoft, revealing high oral bioavailability and GI absorption. SwissTargetPrediction and SuperPred identified protein targets, whereas GeneCards provided OSCC-related targets. A Venn diagram showed 34 overlapping targets between OA and OSCC. STRING and Cytoscape were used to construct a protein-protein interaction (PPI) network with 32 nodes and 164 edges, identifying HSP90AA1, STAT3, HSP90AB1, PI3KR1, and NFKB1 as key hub genes. Gene ontology and KEGG enrichment analyses highlighted relevant biological processes, molecular functions, and pathways. Molecular docking and dynamics simulations confirmed the strong binding of OA to hub targets. Experimental validation showed that OA inhibited cell viability and colony formation in a dose-dependent manner, induced apoptosis, and downregulated HSP90AA1, STAT3, and PI3KR1 proteins. In conclusion, this comprehensive study combining network pharmacology, bioinformatics, molecular simulations, and experimental assays provides valuable insights into OA's anticancer potential and detailed mechanism of action in OSCC.

**Keywords:** oleanolic acid, network-pharmacology, apoptosis, gene-ontology, molecular docking, survival analysis

Accepted February 12, 2025  
Published online February 13, 2025

## INTRODUCTION

Oleanolic acid (OA), a naturally occurring pentacyclic triterpenoid, is widely distributed in several medicinal plants, such as olive leaves, berries, and various other herbs (1). It has been acknowledged for its many pharmacological properties, including anti-inflam-

---

\* Correspondence; e-mail: zouyaqin7865@hotmail.com

matory, antimicrobial, antiviral, hepatoprotective, and anticancer effects (2, 3). In recent years, OA gained significant interest for its potential as a therapeutic agent in cancer treatment, providing a safer and more sustainable alternative to traditional chemotherapy. Its anticancer properties are ascribed to its capacity to block cell proliferation, trigger apoptosis, and regulate many signaling pathways implicated in cancer advancement (4). Research has shown that OA can target many molecular processes, positioning it as a possible option for cancer treatment. The safety profile and bioavailability of OA, together with its capacity to alter critical cancer-related molecular targets, provide a persuasive justification for investigating it as an efficacious natural anticancer drug.

OSCC is the predominant form of oral cancer, constituting over 90 % of all instances (5). It often originates in the epithelial lining of the oral cavity and is strongly linked to risk factors including tobacco use, alcohol intake, human papillomavirus (HPV) infection, and inadequate oral hygiene (6). OSCC is characterized by aggressive proliferation, local invasion, and a significant propensity for metastasis to regional lymph nodes. Notwithstanding progress in surgical methods, radiation, and chemotherapy, the prognosis for patients with OSCC remains unfavorable, especially in late stages, with an overall survival rate of around 50–60 % (7). The complicated molecular etiology of OSCC requires the formulation of innovative treatment approaches. Identifying molecular targets and comprehending the genetic and epigenetic modifications that drive OSCC advancement are essential for enhancing treatment results and developing novel targeted treatments.

Recent breakthroughs in computer-aided drug design (CADD) have markedly improved the capacity to evaluate natural compounds for possible therapeutic uses, including anticancer medicines (8). CADD includes several computational techniques, including molecular docking, network pharmacology, differential gene expression analysis, and gene ontology enrichment, which together facilitate the discovery and optimization of bioactive substances. Molecular docking enables researchers to project the binding affinities and interactions of natural chemicals with designated protein targets, offering insights into their potential effectiveness (9). Network pharmacology provides a comprehensive framework for examining the connections of bioactive chemicals, various targets, and signaling pathways, therefore clarifying the multi-target processes of natural products (10). Differential gene expression analysis is a potent method for elucidating the impact of natural substances on cancer cells at the transcriptional level, identifying genes that are either upregulated or downregulated in response to therapy (11). Integrating this data with Gene Ontology enrichment analysis elucidates the biological processes and molecular functions affected by the chemicals, providing a more profound comprehension of the underlying mechanisms. Collectively, these methodologies enable the identification of potential natural product-derived therapeutic candidates, hence facilitating a more focused strategy in the formulation of treatments for intricate disorders like cancer.

The study aims to investigate the anticancer effects of OA in OSCC by integrating network pharmacology, gene ontology, differential gene expression, survival analysis, molecular docking, and experimental techniques. This approach enables a comprehensive understanding of the multi-target mechanisms of OA, predicting its interactions with key biological targets in OSCC. By combining computational and experimental methods, the study seeks to validate the potential of OA as a natural therapeutic agent for oral cancer treatment.

## EXPERIMENTAL

### *Pharmacokinetic profiling using SwissADME and Molsoft*

The pharmacokinetic properties like oral bioavailability and synthetic accessibility of OA were predicted using the SwissADME web tool (<https://www.swissadme.ch/>) (12). Drug-likeness of OA was analysed using Molsoft (<https://www.molsoft.com/mprop/mprop.cgi>) to predict its solubility, number of hydrogen bond donors and acceptors, and other physicochemical properties (13). These parameters were used to confirm the suitability of OA as a potential therapeutic agent.

### *Target prediction with SwissTargetPrediction and SuperPred*

SwissTargetPrediction (<http://www.swisstargetprediction.ch/>) (14) and SuperPred (<https://prediction.charite.de/>) were employed to identify potential protein targets for OA, based on its chemical structure. The targets were screened with screening criteria for probability, considering  $\geq 60$  % probability significant. This *in silico* prediction provided a list of candidate targets, enabling further exploration of molecular mechanisms for OA.

### *Identification of OSCC-related targets using GeneCards*

To identify relevant therapeutic targets for OSCC, the GeneCards database (<https://www.genecards.org/>) was used to retrieve genes associated with OSCC, focusing on high-relevance scores. The targets were screened on the basis of the Gifts score and a Gifts score  $\geq 60$  was considered significant. This list formed the basis for intersecting OA targets with disease-related targets.

### *Target intersection analysis using Venny*

Common targets between OA-predicted targets and OSCC-related genes were identified using the Venny 2.0.2 tool (<https://bioinfo.p.cnbc.csic.es/tools/venny/index2.0.2.html>), enabling the selection of relevant therapeutic targets for OA in the context of OSCC. These intersecting targets were considered potential mediators of anticancer effects for OA.

### *Network construction and analysis using STRING*

A protein-protein interaction (PPI) network was constructed for the intersecting targets using STRING (<https://string-db.org/>), with a confidence score cut-off of 0.4 to ensure high-quality interactions. The network data were exported for further analysis.

### *Network visualization and hub gene identification with Cytoscape*

The PPI network was visualized using Cytoscape software, and the CytoHubba plugin was applied to identify hub genes. Topological parameters such as degree, closeness, and betweenness centrality were used to rank the top 10 hub genes, focusing on those with the highest scores.

### *Gene ontology and KEGG pathways*

Gene ontology enrichment and KEGG pathway analysis were conducted using the ShinyGo 0.80 platform (<http://bioinformatics.sdstate.edu/go/>). The analysis identified significant enrichments in biological processes (BP), cellular components (CC), molecular functions (MF), and KEGG-enriched pathways.

### *Molecular docking using DockThor*

The binding affinity of OA with the top three hub genes was assessed through molecular docking using CB-Dock2 (<https://cadd.labshare.cn/cb-dock2/index.php>) (15). The 3D structures of target proteins were obtained from the RCSB Protein Data Bank (PDB) database in .pdb format, and OA was docked to evaluate interaction energies, with lower binding energies indicating stronger binding potential. The proteins HSP90AA1, STAT3, and PI3KR1 (PDB IDs: 4U93, 4ZIA, and 7PG5, resp.) were prepared for docking using BIOVIA Discovery Studio by removing water molecules and ligands already present in the structure (16–18). We considered only HSP90AA1 for molecular docking over HSP90AB1 because they exhibit 86 % identity and 93 % similarity. The structure of OA was prepared in .pdb using ChemBio3D Ultra V 11.0 after downloading the structure file from the PubChem database. The interactions between the ligand-protein complexes were visualised using Discovery Studio.

### *Molecular dynamics simulations using iMODS and CABS-Flex*

Molecular dynamics (MD) simulations were performed using iMODS (<https://imods.iqf.csic.es/>) (19) and CABS-Flex (20) (<https://biocomp.chem.uw.edu.pl/CABSflex2/index>) to evaluate the docked OA-target complexes' stability and dynamic behaviour. Protein-ligand complexes were tested for structural flexibility and deformability using iMODS for normal mode analysis. After that, the protein's backbone dynamics were modelled using CABS-Flex in a near-native environment. This allowed us to understand the stability of the complexes and changes in conformation.

### *Chemicals and cell cultures*

All chemicals used in this study were of high-quality grade procured from Sigma Aldrich, USA. Cancer cells Cal-27 and normal oral epithelial cells HaCaT (Cell Resource Center of Shanghai Institutes for Biological Sciences, Chinese Academy of Sciences, China) were cultured in a complete medium (Dulbecco's modified eagle medium) supplemented with 10 % FBS and 1 % antibiotics. Cells were maintained in a humidified incubator at 37 °C with 5 % CO<sub>2</sub>. For experiments, cells were seeded at appropriate densities and allowed to adhere overnight before the introduction of treatments.

### *MTT assay for cell viability*

Cells were treated with increasing concentrations of oleanolic acid (0, 25, 50, 75, and 100 μmol L<sup>-1</sup>) for 24 hours. After the treatment period, MTT solution (5 mg mL<sup>-1</sup>) was added to each well and incubated at 37 °C for 4 hours. Formazan crystals were dissolved

in dimethyl sulfoxide (DMSO), and the absorbance was measured at 570 nm using a microplate reader. Cell viability was calculated as a percentage relative to untreated control cells.

### *Colony formation assay*

For evaluating long-term cell proliferation, cells were plated at a low density (500–1000 cells per well) in 6-well plates and treated with oleanolic acid (0, 25, 75, and 100  $\mu\text{mol L}^{-1}$ ) for 14 days. Colonies were fixed with methanol and stained with crystal violet. Colonies with at least 50 cells were counted under a light microscope (Olympus, Japan), and the results were expressed as a percentage of colony numbers compared to the untreated control.

### *Annexin V assay for apoptosis detection*

Apoptosis was assessed using flow cytometry. Cells were exposed to oleanolic acid (0, 25, 75, and 100  $\mu\text{mol L}^{-1}$ ) for 24 hours. Treated cells were harvested, washed with PBS, and stained with annexin V-FITC and propidium iodide following the kit instructions (Keygen, China). The proportion of live, early apoptotic, and late apoptotic/necrotic cells was determined by flow cytometry (Becton Dickinson, USA).

### *Western blot analysis for HSP90AA1, STAT3 and PI3KR1*

To assess protein expression for HSP90AA1, STAT3, and PI3KR1, cells treated with oleanolic acid (0, 25, 75, and 100  $\mu\text{mol L}^{-1}$ ) for 24 hours were lysed in a buffer containing protease and phosphatase inhibitors. Protein concentrations were quantified using a Bradford assay. Equal protein amounts (30  $\mu\text{g}$ ) were separated by SDS-PAGE and transferred onto PVDF membranes. After blocking with 5 % non-fat milk, membranes were incubated overnight with primary antibodies against HSP90AA1, STAT3, and PI3KR1 (1:1000 dilution) at 4 °C. The membranes were then incubated with HRP-conjugated secondary antibodies and developed using enhanced chemiluminescence (ECL) reagents. Band intensities were quantified using ImageJ software, with GAPDH used as a loading control.

### *Statistical analysis*

The data were analysed by GraphPad Prism Software, Version 5.0 (GraphPad Software, Inc., USA) and represented as mean  $\pm$  SD; the statistical analysis was performed by one-way ANOVA followed by Turkey's comparison test. Statistical differences between different groups were defined at  $p < 0.05$ .

## RESULTS AND DISCUSSION

### *Pharmacokinetic study and target identification*

An overview of the complete study design and methods adopted in the current study is presented in Fig. 1. OA shows favorable pharmacokinetic properties, with a high oral bioavailability score indicating good absorption potential. Its lipophilicity supports mem-

Table I. Physicochemical parameters of OA assessed with SwissADME and Molsoft tools

Oleanolic acid – physicochemical parameters	
$M_r$	456.36
Number of HBA	3
Number of HBD	2
Mol logP	6.66 (> 5)
Mol logS	-5.63 (log mol L <sup>-1</sup> ); 1.07 (mg L <sup>-1</sup> )
Mol PSA	44.14 Å <sup>2</sup>
Mol Vol	593.27 Å <sup>3</sup>
pK <sub>a</sub> of most basic/acidic group	< 0. / 5.73
BBB Score	3.68
Number of stereo centers	8
Oral bioavailability	0.85
Drug-likeness model score	0.37

BBB – blood-brain barrier,  $M_r$  – molecular mass, HBA – hydrogen bond acceptors, HBD – hydrogen bond donors, Mol logP – molecular log partition coefficient, Mol logS – molecular log solubility, Mol PSA – molecular polar surface area, Mol Vol – molecular volume, pK<sub>a</sub> – negative logarithm of the acid dissociation constant

brane permeability, whereas moderate polar surface area suggests a balanced ability to interact with biological targets (Table I).

A total of 100 possible targets for OA were found using SwissTarget Prediction and 3 confirmed targets and 53 possible targets were identified using SuperPred; 62 of these showed a probability of ≥ 60 % after removing the duplicates (Table SI). Concurrently, the GeneCards database provided 10,093 targets linked to OSCC, out of which only 935 survived the threshold for Gifts score (Table SII). By the use of Venny 2.0.2, the junction of these datasets produced 34 shared targets between OA and OSCC (Fig. 2a and Table II).

Table II. The common genes shared between oleanolic acid biological targets and targets in oral squamous carcinoma

Intersecting targets			
BLM	HSP90AA1	CDK5	CACNA1B
PDGFRA	TOP2A	TLR8	SCN3A
TERT	CTSD	GBA1	PDE3A
AR	AURKB	SLC9A1	PTPRF
STAT3	KDM1A	CSNK2B	
PIK3R1	HSP90AB1	RPS6KA1	
NFKB1	ITK	HSD11B1	
NTRK3	ADAM10	GRIN1	
TLR4	PTPN1	PDE4D	
CYP3A4	NR4A1	SCN2A	

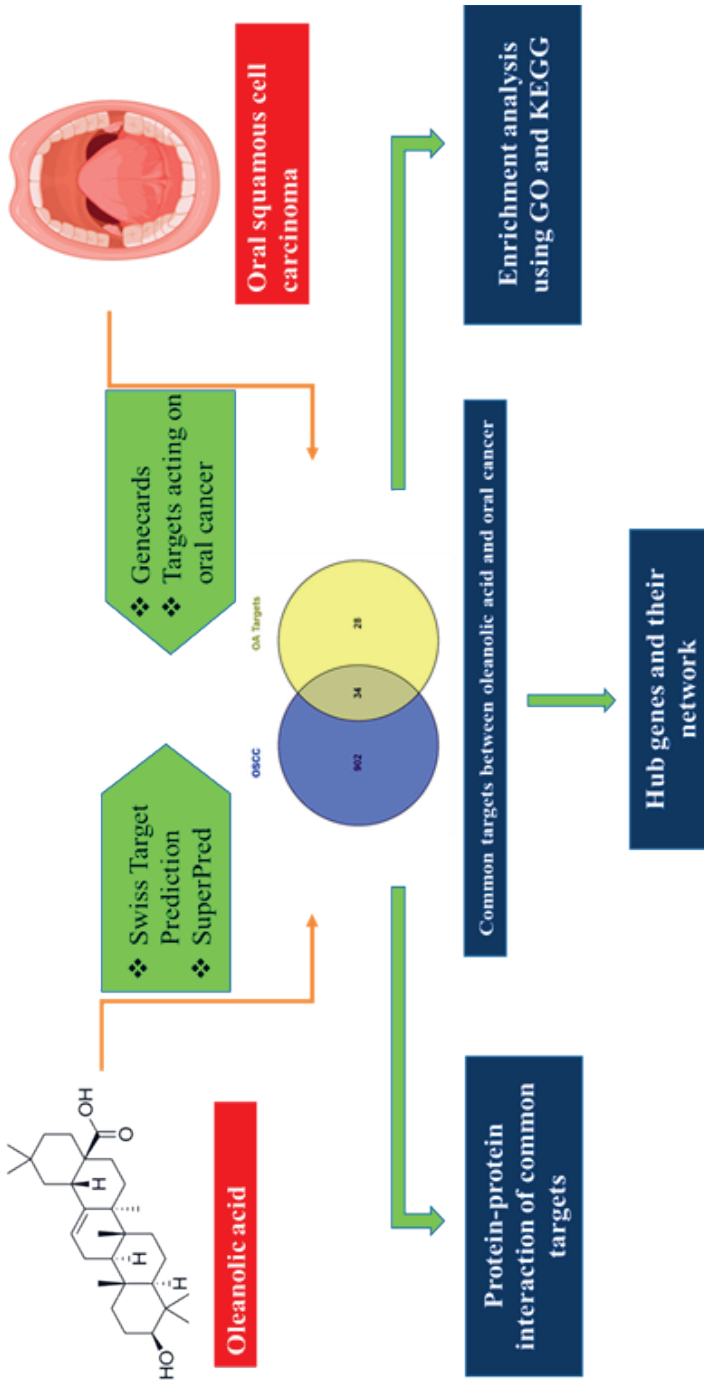


Fig. 1. Overall study design using multi-method computational, network pharmacology, *in silico* molecular docking and dynamics simulations, and experimental assays for demonstrating the anticancer effects of oleanolic acid and its detailed mechanism in oral squamous carcinoma cells.

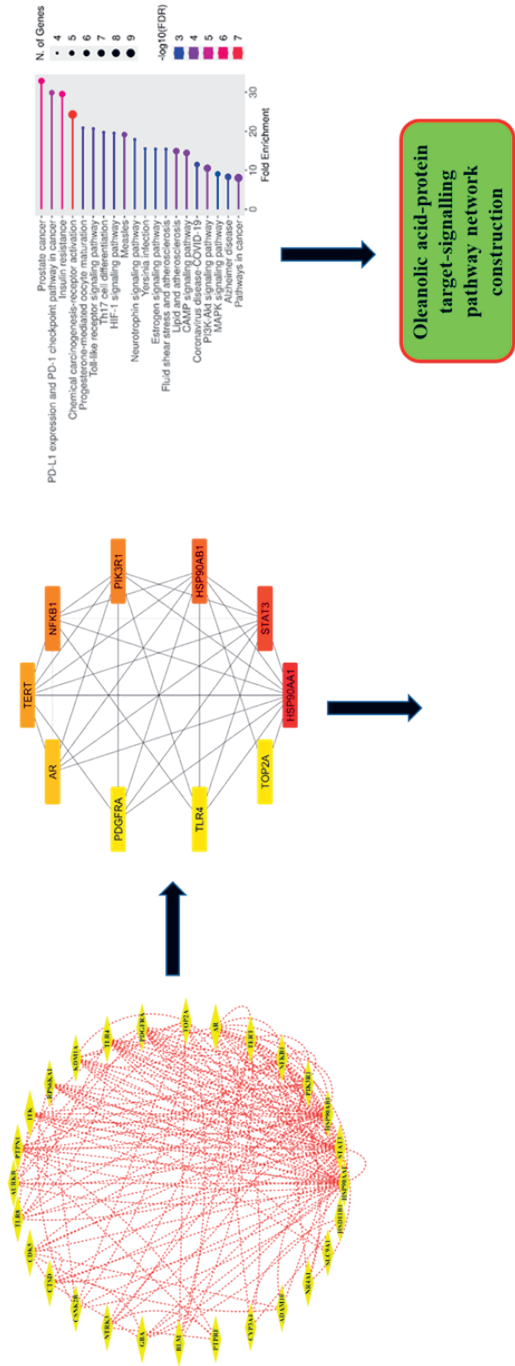


Fig. 1. Continued.

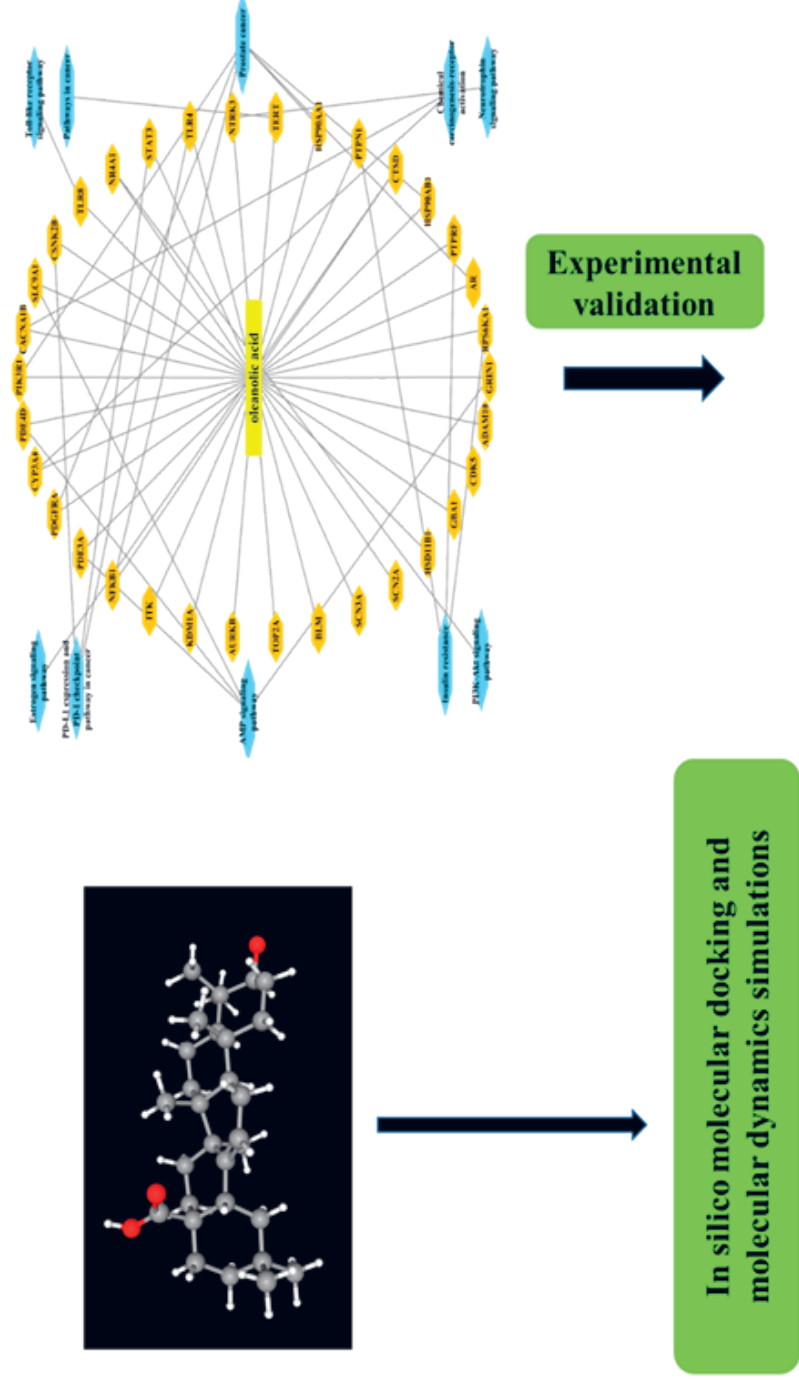


Fig. 1. Continued.

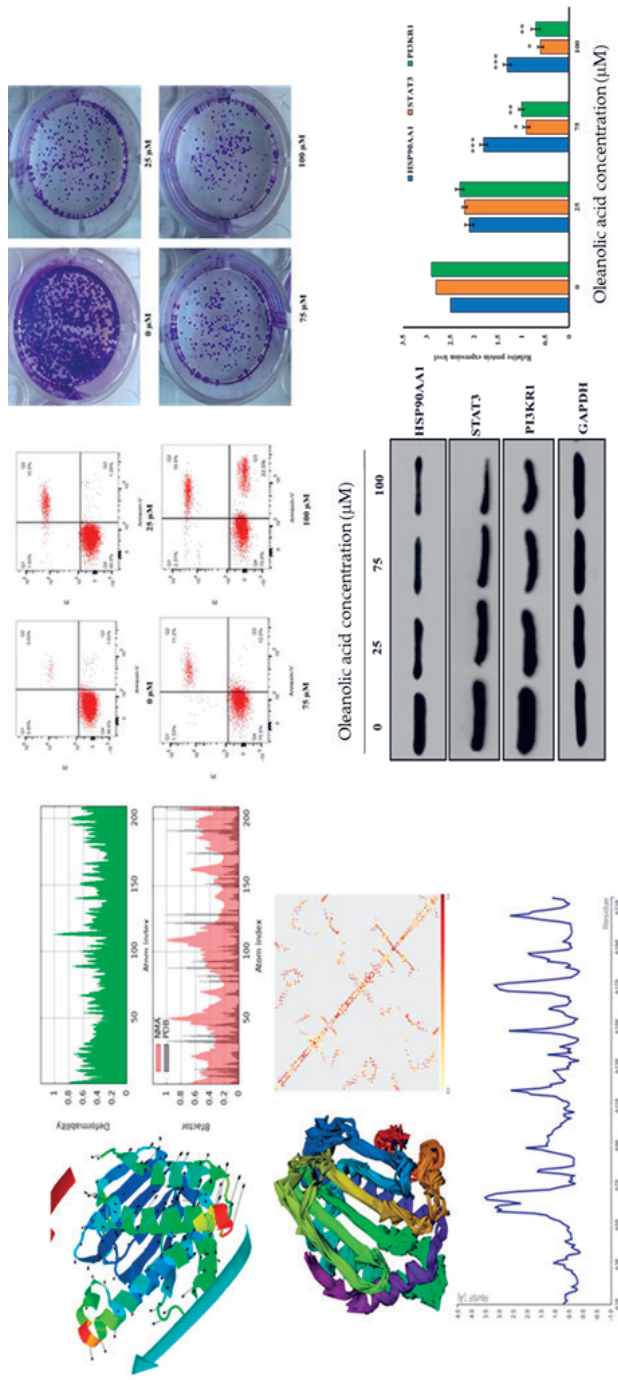


Fig. 1. Continued.

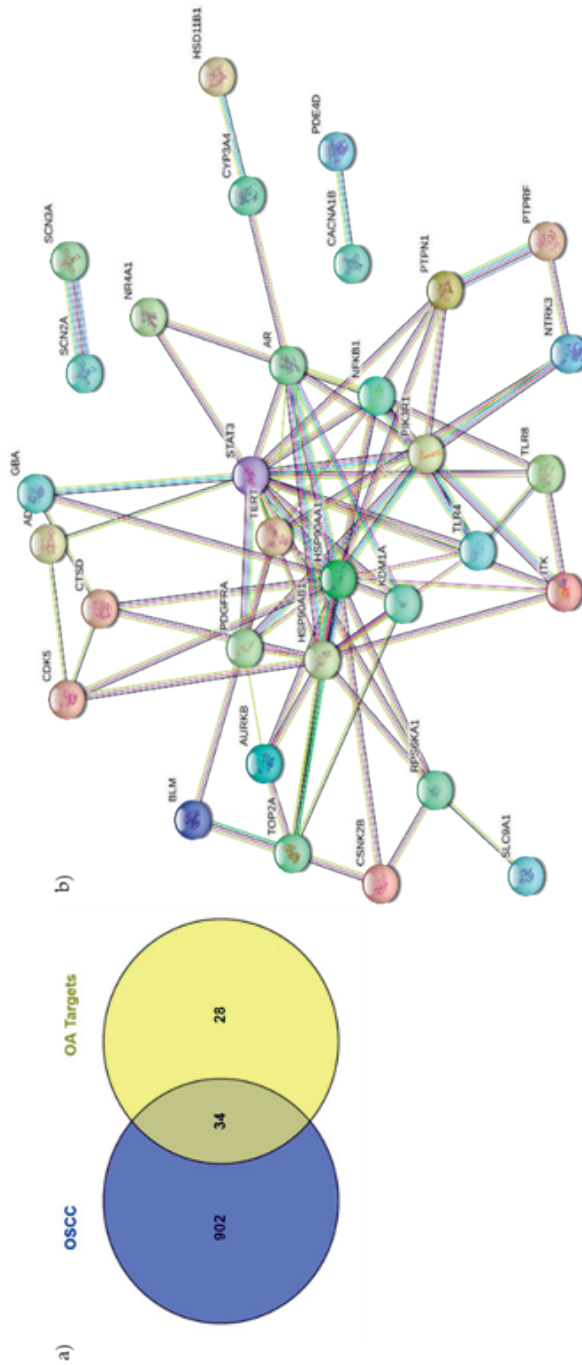


Fig. 2. a) Venn diagram illustrating the intersection of OA targets identified by SwissTargetPrediction and SuperPred and OSCC-related targets from GeneCards, revealing 34 common targets; b) protein-protein interaction (PPI) network constructed for the intersecting targets between OA and OSCC, displaying the relationships among the proteins; c) visualization of the PPI network in Cytoscape, featuring 28 nodes and 160 edges representing interactions among the identified targets; d) Top 10 hub proteins with the highest PPI connectivity, including HSP90AA1, STAT3 and PIK3R1 based on their interaction counts.

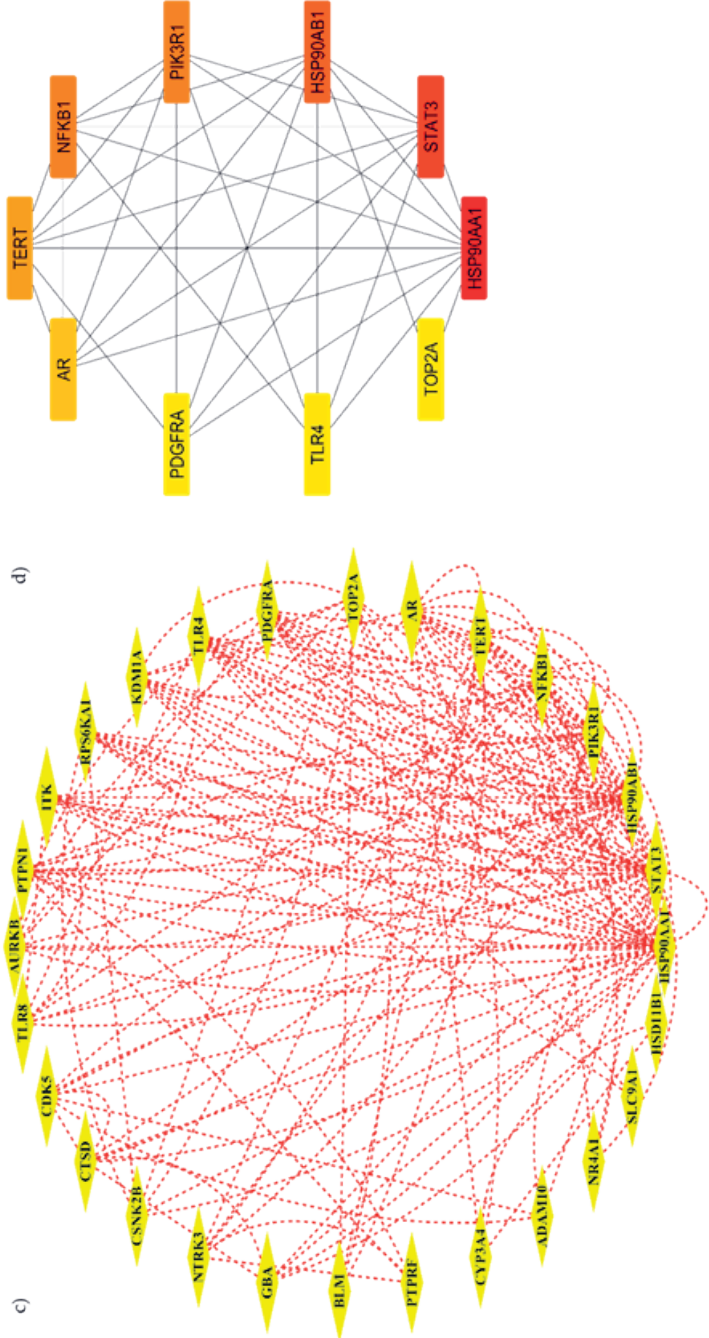


Fig. 2. Continued

### PPI network construction and analysis

Using the STRING database, a PPI network was built for the intersection of OA and OSCC with a confidence score threshold of 0.40 (Fig. 2b). The string network contained 32 nodes and 164 edges. Subsequently, the network was downloaded and presented in Cytoscape to show the 28 nodes and 160 edges (Fig. 2c). The analysis of this network using the Cytohubba plugin in Cytoscape led to the identification of the top 10 genes with the highest PPI connectivity by implementing degree method. The genes include HSP90AA1, STAT3, HSP90AB1, PIK3R1, NFKB1, TERT, AR, PDGFRA, TOP2A, and TLR4 with interactions scores as 36, 32, 28, 20, 20, 18, 16, 12, 12, and 12, resp. (Fig. 2d).

### Gene ontology and KEGG results

The GO enrichment analysis highlights significant BP, CC, and MF involved in OSCC. Key BPs include the regulation of protein serine/threonine phosphatase activity, phosphorylation, and activation receptor signalling, which are crucial for cellular signalling and metabolic control. Processes such as endothelial morphogenesis and response to endogenous and chemical stimuli underscore roles in vascular development and homeostasis (Fig. 3a). In CC, enriched terms involve vesicular structures like the ficolin-1-rich granule lumen and secretory granule lumen, reflecting functions in secretion and intracellular transport. Protein complexes, including the cation channel complex and transporter complex, indicate roles in molecular transport, while intracellular components like the nucleoplasm and nuclear lumen suggest involvement in transcription and chromatin regulation (Fig. 3b). In MF, activities such as protein kinase regulator activity, serine/threonine kinase activity, and chromatin binding highlight regulation of signaling pathways, transcription, and enzymatic functions, with additional roles in binding and molecular interactions (Fig. 3c).

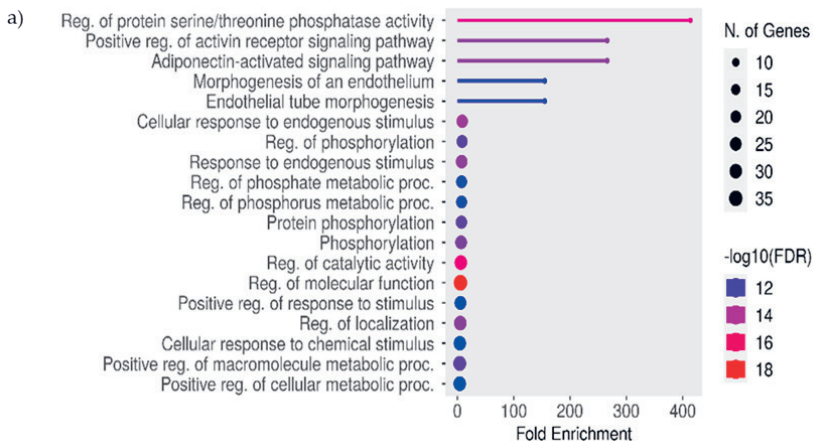


Fig. 3. Gene ontology (GO) analysis results showing significant enrichment in: a) BP; b) CC; c) MF; d) shows KEGG enrichment analysis results indicating key signalling pathways associated with the overlapping genes, including MAPK and PI3K-Akt signaling, insulin resistance, and chemical carcinogenesis-receptor activation, as well as cancer-specific pathways like PD-L1 expression, PD-1 checkpoint pathway, and pathways in cancer.

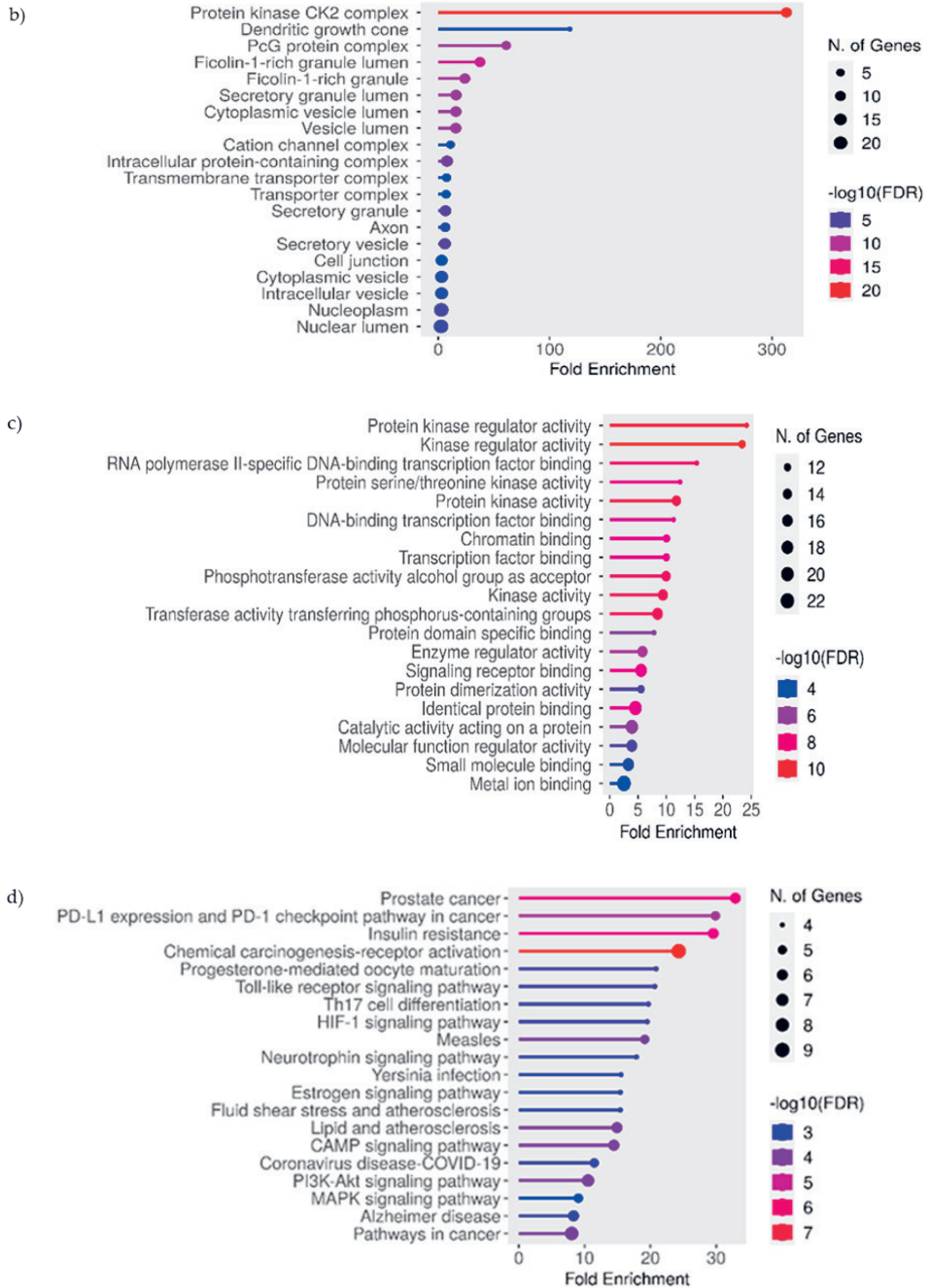


Fig. 3. Continued.

KEGG pathway enrichment reveals associations with diverse biological contexts, including cancer-related signalling pathways like PI3K-Akt, MAPK, and the PD-L1 checkpoint, highlighting the gene set's involvement in tumorigenesis and immune evasion. Pathways such as insulin resistance, fluid shear stress, and lipid metabolism underscore metabolic regulatory roles. Immune-related pathways like Toll-like receptor signalling and Th17 cell differentiation suggest immunomodulatory functions (Fig. 3d). KEGG pathway analysis revealed involvement of OA in critical cancer-related pathways such as PI3K-Akt, MAPK, and PD-L1 checkpoint, which regulate tumor survival, immune evasion and metastasis (21–23). The potential of OA to modulate these pathways suggests it could inhibit tumor growth and immune escape mechanisms in OSCC. The gene mapping flowcharts corresponding to the PD-1/PDL1 checkpoint pathway in cancer and cancer pathways is shown in Figs. 4a and 4b, resp. A common network revealing the interactions

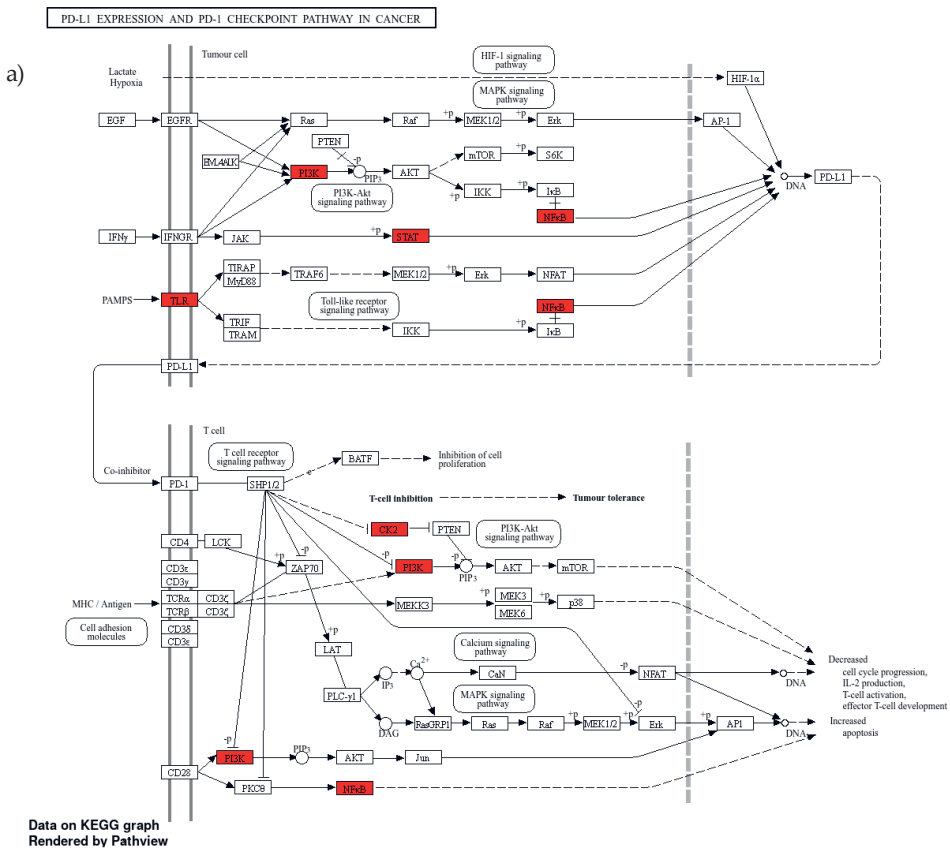


Fig. 4. a) Gene mapping showing the common genes between the biological targets of oleanolic acid and the gene targets in oral squamous cell carcinoma involved in the PD-L1 expression and PD-1 checkpoint pathway in cancer; b) gene mapping showing the common genes between the biological targets of oleanolic acid and the genes in oral squamous cell carcinoma are involved in various cancer-related pathways.



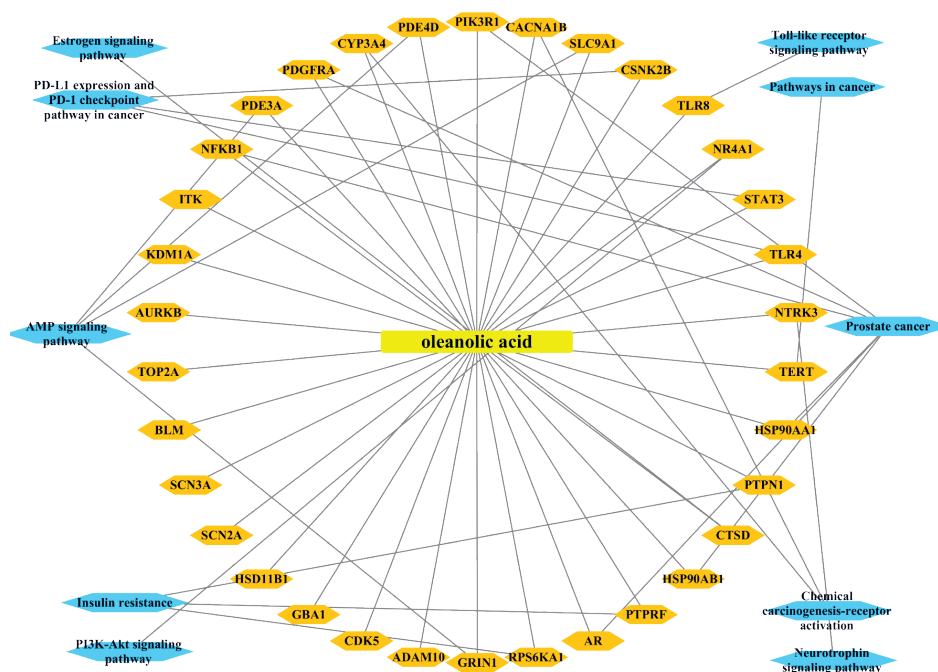


Fig. 5. Construction of compound-target-signalling pathway enrichment network representing significant interactions with 45 nodes and 57 edges. The octagon in the centre shows oleanolic acid followed by circles which display protein targets and at the periphery of the network in diamond shape are the signalling pathways involved.

between oleanolic acid, target genes, and pathways in which target genes are enriched was developed by using Cytoscape with 45 nodes and 57 edges (Fig. 5a).

### Docking validation

The CB-Dock2 docking analysis results provide insights into the binding interactions of OA with HSP90AA1, STAT3, and PI3KR1 (Table III). For OA-HSP90AA1, docking occurred in cavity C1 with a Vina score of  $-8.9$ , indicating strong binding affinity. The cavity volume was  $1671 \text{ \AA}^3$ , and the docking box with center coordinates  $x = 27$ ,  $y = 24$ , and  $z = 11$ , and size

Table III. Molecular docking results of OA with top 3 hub genes including HSP90AA1, STAT3, and PI3KR1, using the CB-Dock2 online tool

Docked complex	CurPocket ID	Vina score	Cavity volume ( $\text{\AA}^3$ )	Center ( $x, y, z$ )	Docking size ( $x, y, z$ ) ( $\text{\AA}$ )
OA-HSP90AA1	C1	$-8.9$	1671	27, 24, 11	26, 20, 20
OA-STAT3	C3	$-8.5$	884	81, 60, 125	20, 20, 20
OA-PI3KR1	C3	$-10.1$	6490	11, $-31$ , 32	28, 35, 26

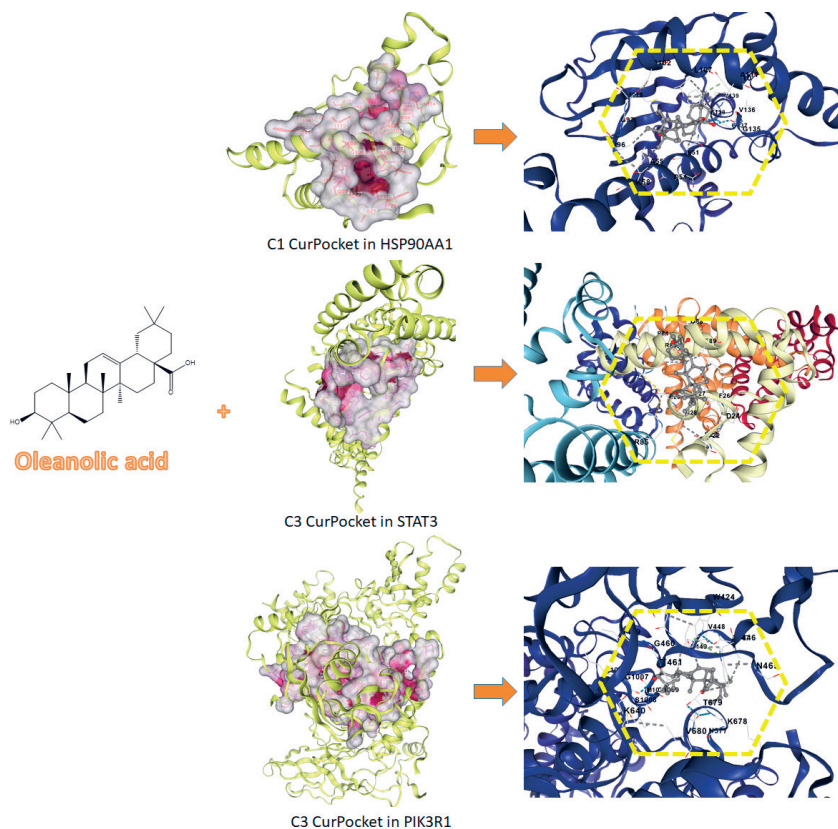


Fig. 6. Molecular docking analysis of the OA-HSP90AA1, OA-STAT3, and OA-PIK3R1 complex showing the binding affinity and interaction types, illustrating the strength of their interaction.

coordinates  $x = 26 \text{ \AA}$ ,  $y = 20 \text{ \AA}$ , and  $z = 20 \text{ \AA}$ . The binding pocket involves several key residues, such as ASN51, ASP54, ALA55 and TYR139, which likely contribute to the compound's stable interaction with the protein (Fig. 6). For OA-STAT3, docking in cavity C3 yielded a Vina score of  $-8.5$  and a smaller cavity volume of  $884 \text{ \AA}^3$  with center and size coordinates  $x = 81$ ,  $y = 60$  and  $z = 125$ , and  $x = 20 \text{ \AA}$ ,  $y = 20 \text{ \AA}$ ,  $z = 20 \text{ \AA}$ , resp. Interacting residues include TYR22, PHE26 and MET28 on chain C and ARG85 on both chains C and D (Fig. 6). For OA-PIK3R1, docking in cavity C3 achieved the highest Vina score of  $-10.1$ , indicating a very strong binding. The cavity volume was  $6490 \text{ \AA}^3$ , with center and size coordinates  $x = 11$ ,  $y = -31$  and  $z = 32$  and  $x = 28 \text{ \AA}$ ,  $y = 35 \text{ \AA}$ , and  $z = 26 \text{ \AA}$ , resp. Key residues like ARG88, GLU116, and ASP743 are involved, suggesting potential inhibition of PI3K signalling, a pathway central to cancer cell growth and survival (Fig. 6).

### Molecular dynamics

The iMODS study of OA complexes with HSP90AA1 (Fig. 7a), STAT3 (Fig. 7b), and PIK3R1 (Fig. 7c) showed changes in deformities and beta factor, revealing the stability and

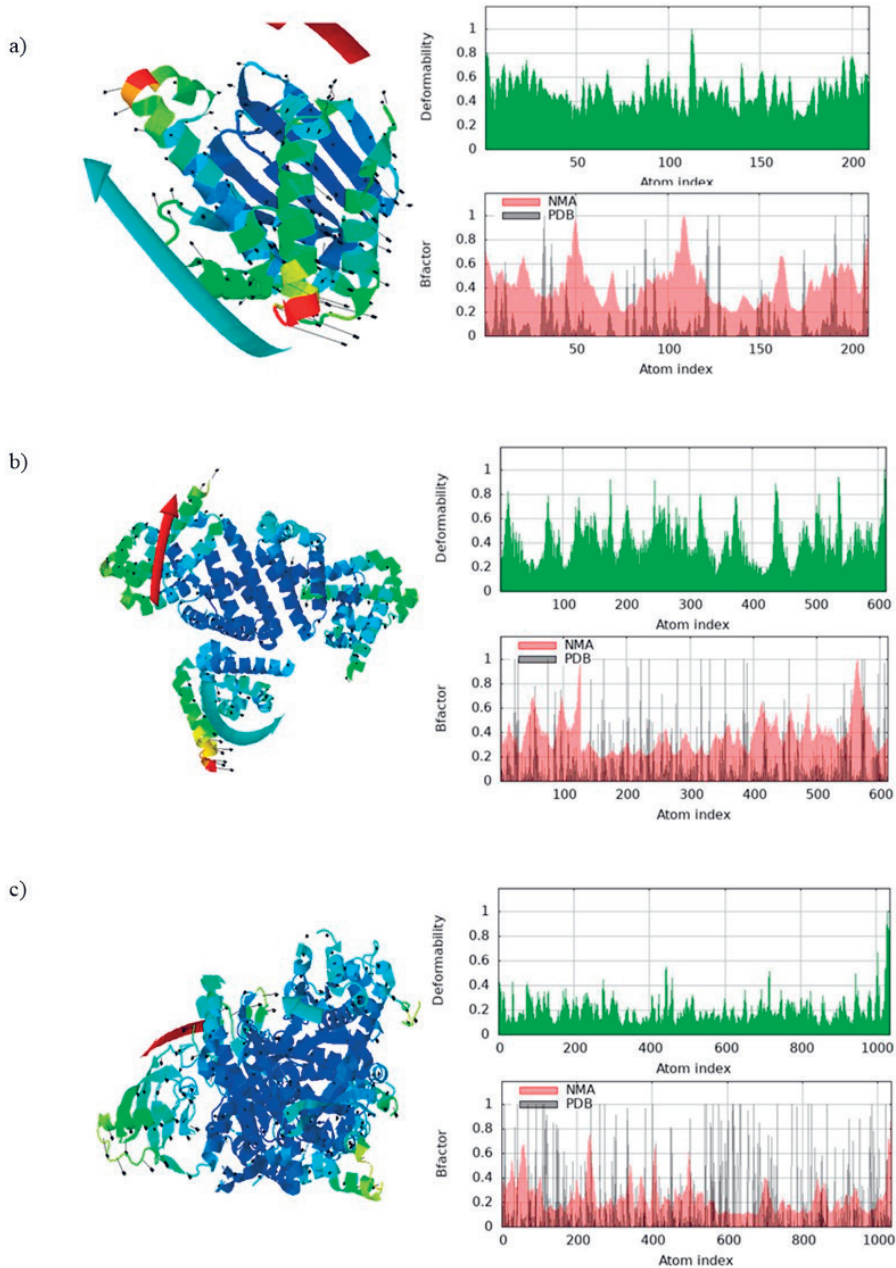


Fig. 7. a) iMODS analysis of the OA-HSP90AA1 complex showing deformity and beta factor, indicating stability and flexibility; b) iMODS analysis of the OA-STAT3 complex, revealing structural dynamics and stability metrics; c) iMODS analysis of the OA-PI3KR1 complex, illustrating the flexibility and deformability of the protein-ligand interaction.

flexibility of these protein-ligand interactions. The RMSF of three complexes and contact maps were assessed using CABS-flex. RMSF analysis showed flexibility in each complex, whereas contact maps showed critical residue interactions and probable conformational changes (Figs. 8a–c).

### *Inhibition of cell proliferation and colony formation*

The MTT assay results demonstrated that OA induced concentration-dependent cytotoxicity in Cal-27 oral cancer cells after 24 hours, with significantly higher effects compared to HaCaT normal cells, indicating detectable selectivity for cancer cells but still too modest

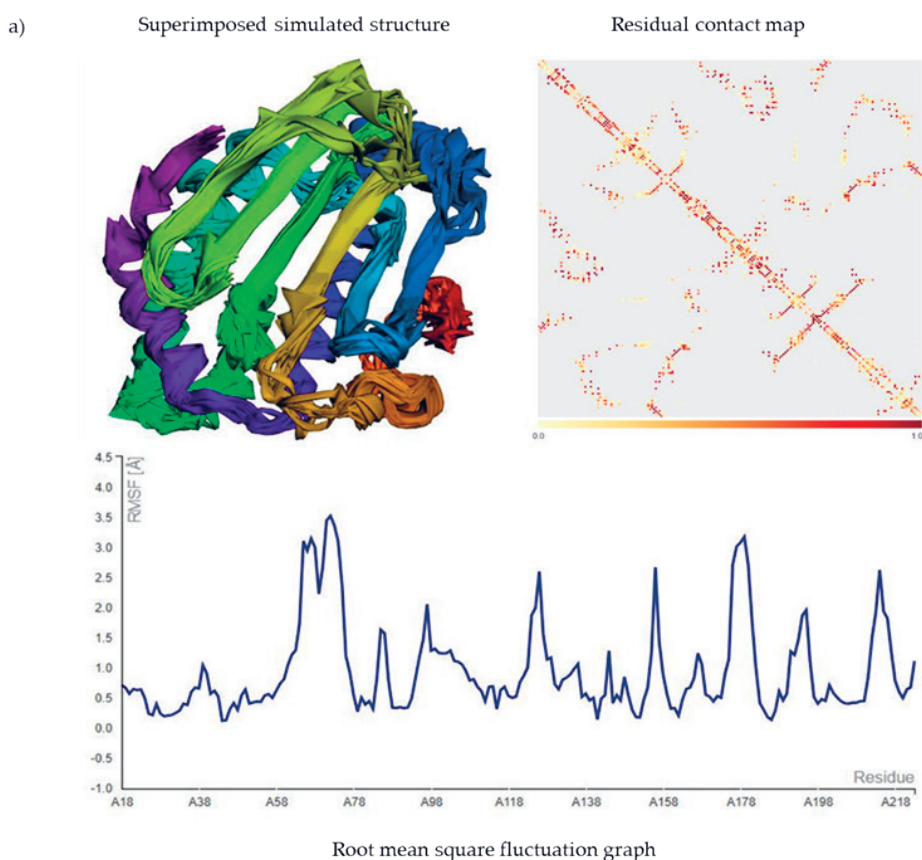


Fig. 8. Structural and dynamic analysis of OA-hub gene docked complexes using CABS-flex online simulation tool. The multimodel superimposed simulated structures illustrate the conformational flexibility of the protein-ligand complexes, while the contact maps highlight key residue interactions. RMSF analysis reveals flexible and stable regions, indicating crucial sites for ligand binding and protein dynamics. a) OA-HSP90AA1, b) OA-STAT3, c) OA-PI3KR1.

selectivity index of 1.70 (Fig. 9a). Additionally, OA inhibited colony formation in Cal-27 cells in a concentration-dependent manner (Figs. 9b,c), revealing its cell colony inhibitory effects in OSCC cells. These findings suggest that OA selectively targets cancer cells while minimizing toxicity to normal cells, supporting its potential as a therapeutic agent for OSCC treatment.

### Apoptotic cell death

Flow cytometry results from the Annexin V/PI assay indicated that OA induces apoptotic cell death in Cal-27 cells. As OA concentration increased, a corresponding rise in early (Q2) and late apoptotic (Q3) cell populations was observed, while the viable cell population (Q4) decreased, demonstrating OA's dose-dependent pro-apoptotic effect (Fig. 10a). Notably, after OA treatment, the percentage of apoptotic cells reached 41.4 %, accompanied by a small necrotic population of 2.3 % (Q1), indicating that apoptosis is the predominant mode of cell death induced by OA in Cal-27 oral cancer cells.

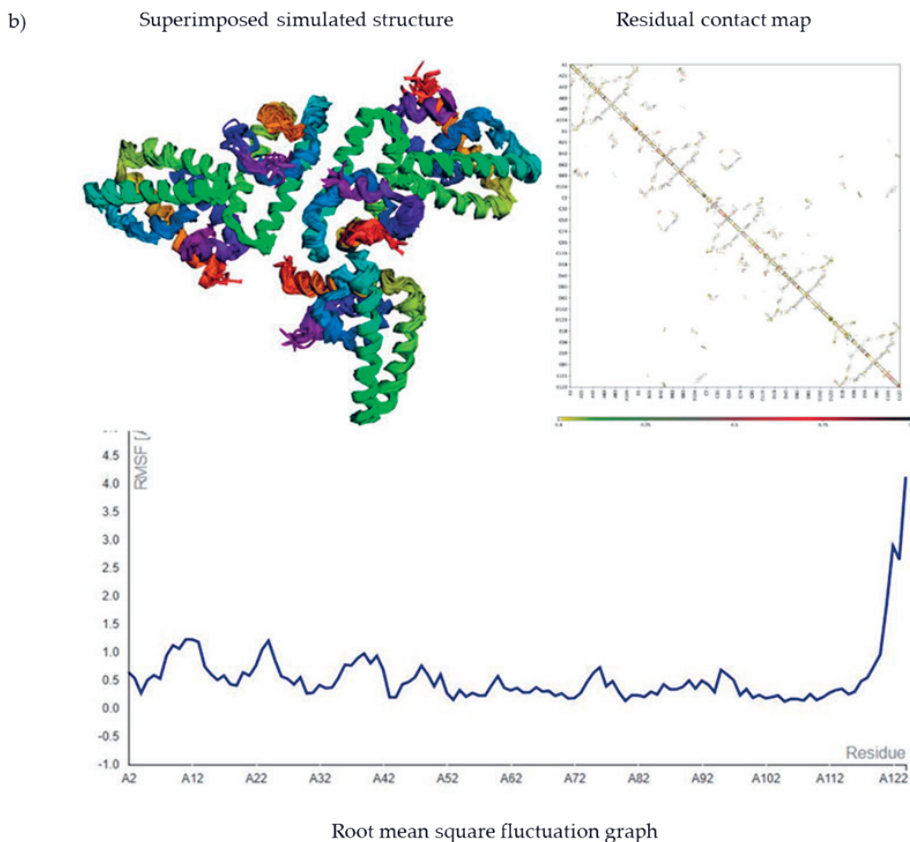


Fig. 8. Continued

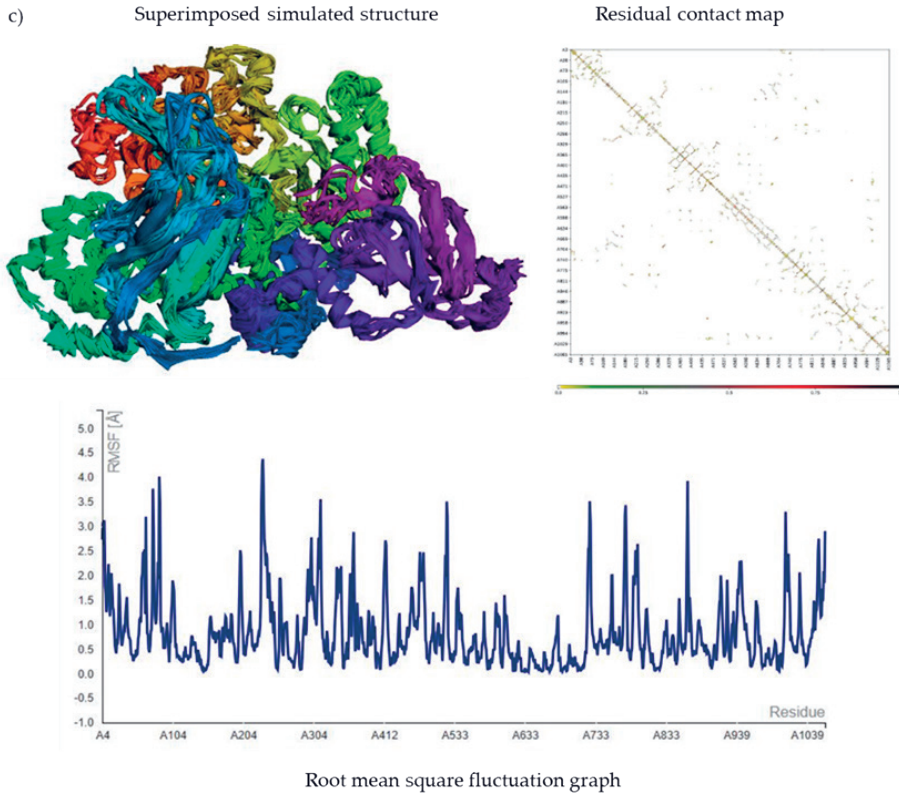


Fig. 8. Continued

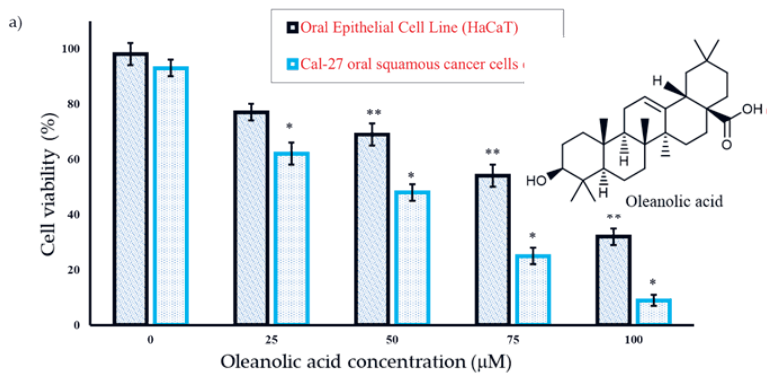


Fig. 9. a) Cytotoxicity of OA in Cal-27 OSCC cells compared to HaCaT normal cells; b) and c) microscopic images and graphical representation of the colony formation assay showing the inhibitory effect of OA on the colony formation of Cal-27 cells. Each bar shows as mean  $\pm$  SD. Significant difference *versus* control group: \* $p < 0.05$ , \*\* $p < 0.01$ , and  $n = 3$ .

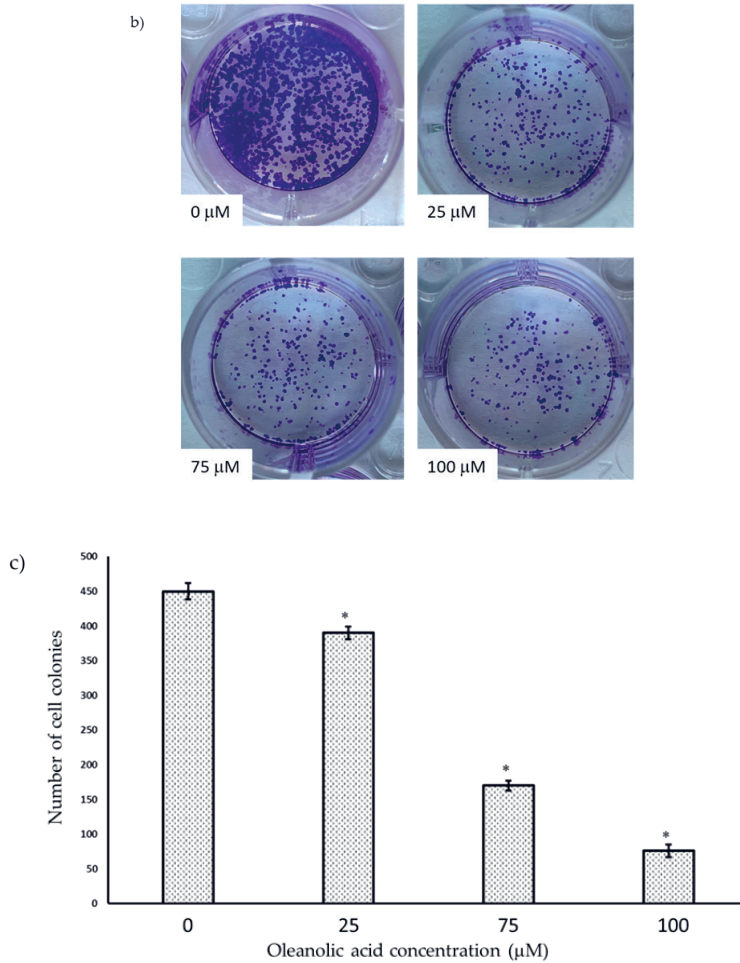


Fig. 9. Continued.

### *Effect of OA on the key protein expressions*

Western blotting analysis was performed to validate network pharmacology, bioinformatics, and *in silico* molecular docking and dynamics studies which indicated that three hub proteins including HSP90AA1, STAT3, and PI3KR1 were actively involved in the anti-cancer mode of action of oleanolic acid in OSCC. Results indicated that increasing concentrations of oleanolic acid led to a significant reduction in the protein expressions of all these three hub protein targets. The expression of PI3KR1 and STAT3 particularly showed more significant and pronounced downregulation as compared to the HSP90AA1 target protein. As compared to the untreated control, the OA-treated cells showed a significant decrease in protein expression. The densitometric analysis showed a graphical representa-

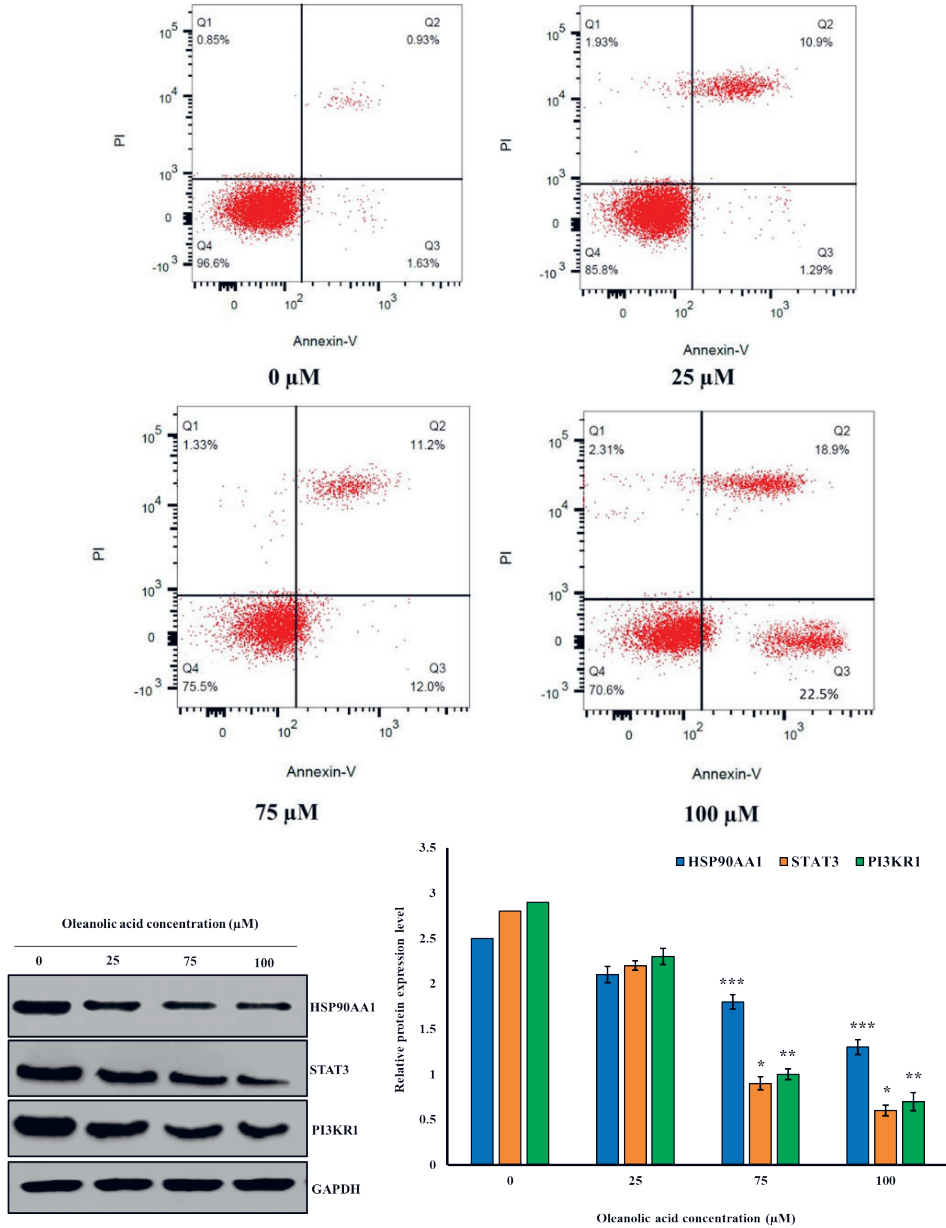


Fig. 10. a) Flow cytometry results from Annexin V/PI assay showing increased early and late apoptotic cell populations in Cal-27 cells after OA treatment; b) Western blot analysis displaying HSP90AA1, STAT3, and PI3KR1 expression in Cal-27 *vs.* control cells; c) quantitative estimation of Western blot intensities for HSP90AA1, STAT3, and PI3KR1 in response to OA concentration in OSCC cells. Each bar shows mean  $\pm$  SD. Significant differences *vs.* control: \* $p < 0.05$ , \*\* $p < 0.01$ , \*\*\* $p < 0.001$ ,  $n = 3$ .

tion of the decrease in protein expression of these three protein targets (Figs. 10b,c). The GAPDH was used as a loading control. The observed decrease in protein expression may also be attributed to indirect mechanisms such as the potential influence of OA on upstream regulatory factors, including transcription factors or signaling pathways. Further studies are required to elucidate whether this downregulation is mediated by direct inhibition of transcriptional or post-transcriptional mechanisms.

HSP90AA1 is a molecular chaperone that plays a pivotal role in cancer progression (24). It stabilizes a variety of proteins involved in critical cellular processes such as signal transduction, cell cycle regulation, and apoptosis (25). In cancers like OSCC, HSP90AA1 helps in the maintenance of oncogenic proteins, including mutant p53 and BRAF, making it a prime target for cancer therapies (26). HSP90AA1 overexpression correlates with poor prognosis, and its inhibition has been shown to reduce tumor growth, induce cell cycle arrest, and enhance apoptotic cell death in different cancers (27). Given its central role in stabilizing multiple oncoproteins, HSP90AA1 represents a significant target for the development of anticancer drugs, especially in OSCC.

STAT3 is another critical oncogene in OSCC (28). In normal cells, STAT3 activation is tightly regulated, but in cancer, particularly OSCC, STAT3 is often constitutively active, driving processes such as cell proliferation, survival, and immune evasion (29). This aberrant activation of STAT3 results in the transcription of genes promoting tumor progression, angiogenesis, and metastasis. In OSCC, overexpression of STAT3 is linked to poor prognosis and resistance to chemotherapy (30). Targeting STAT3 could inhibit these malignant processes, making it a potential therapeutic target in OSCC treatment strategies.

HSP90AB1 shares similar functional roles with HSP90AA1, but it is more involved in regulating steroid hormone receptors and intracellular signalling pathways (31). HSP90AB1 is implicated in various cancers, where it contributes to tumor progression by stabilising client proteins involved in survival pathways (32). It also plays a crucial role in regulating the epithelial-to-mesenchymal transition (EMT), a key event in cancer metastasis (33). As a molecular chaperone, targeting HSP90AB1 could disrupt the stability of oncogenic proteins and suppress tumor growth and metastasis in OSCC.

PI3KR1 is a vital component of the PI3K signalling pathway, which is often dysregulated in cancer (34). The PI3K-Akt pathway is involved in numerous cellular processes, including metabolism, growth, survival, and motility. In OSCC, aberrant activation of PI3KR1 promotes tumorigenesis by enhancing cell survival and proliferation while inhibiting apoptosis (35). It also facilitates metastasis by promoting epithelial-to-mesenchymal transition (EMT) (36). Given the critical role of PI3KR1 in cancer progression, targeting this pathway offers a promising therapeutic approach for OSCC, potentially reversing resistance to chemotherapy and inhibiting metastasis.

## CONCLUSIONS

This study reveals that OA exhibits significant anticancer potential against OSCC by targeting key hub genes like HSP90AA1, STAT3, and PI3KR1. OA showed high oral bioavailability, inhibited cell viability and colony formation, and promoted apoptosis in OSCC cells. Molecular docking and dynamics simulations confirmed the strong binding of OA to hub targets, while bioinformatics analyses highlighted its involvement in critical

cancer-related pathways. The findings provide valuable insights into OA's mechanism of action, supporting its potential use as a therapeutic agent for OSCC.

Supplementary data are available upon request.

*Acronyms, abbreviations, codes.* – ANOVA – analysis of variance, CABS-Flex – C-alpha, beta, and side-chain flexibility, CB-Dock2 – cavity-based docking 2, CADD – computer-aided drug design, DMSO – dimethyl sulfoxide, ECL – enhanced chemiluminescence, FBS – fetal bovine serum, FITC – fluorescein isothiocyanate, GAPDH – glyceraldehyde 3-phosphate dehydrogenase, HSP90AA1 – heat shock protein 90 alpha family class A member 1, HSP90AB1 – heat shock protein 90 alpha family class B member 1, HPV – human papillomavirus, HRP – horseradish peroxidase, iMODS – internal coordinates normal mode analysis server, KEGG – Kyoto encyclopedia of genes and genomes, MTT – 3-(4,5-dimethylthiazol-2-yl)-2,5-diphenyltetrazolium bromide, NFkB1 – nuclear factor kappa B subunit 1, OA – oleanolic acid, OSCC – oral squamous cell carcinoma, PBS – phosphate-buffered saline, PI – propidium iodide, PI3KR1 – phosphoinositide-3-kinase regulatory subunit 1, PPI – protein-protein interaction, PVDF – polyvinylidene difluoride, RCSB Protein Data Bank – Research collaborative for structural bioinformatics protein data bank, SDS-PAGE – sodium dodecyl sulfate polyacrylamide gel electrophoresis, STAT3 – signal transducer and activator of transcription 3, SwissADME – Swiss absorption, distribution, metabolism, and excretion.

*Acknowledgements.* – We would like to express our acknowledgment to all the participating laboratories of our institute involved in data collection of various experiments and computational chemistry/computational biology studies.

*Conflict of interest.* – The authors declare no conflict of interest.

*Funding.* – Funding for this study was provided by the Research on the training incentive mechanism of double-qualified teachers in vocational colleges under the "double-high" plan (The Funding Number: SXSZJS2023SX0024).

*Authors contributions.* – Conceptualization, T.Y. and H.W.; methodology, T.Y. and Y.Z.; analysis, T.Y. and H.W.; investigation, T.Y., H.W. and Y.Z.; writing, original draft preparation, T.Y.; writing, review and editing, H.W. and Y.Z. All authors have read and agreed to the published version of the manuscript.

## REFERENCES

1. E. Gudoityte, O. Arandarcikaite, I. Mazeikiene, V. Bendokas and J. Liobikas, Ursolic and oleanolic acids: Plant metabolites with neuroprotective potential, *Int. J. Mol. Sci.* **22**(9) (2021) Article ID 4599 (15 pages); <https://doi.org/10.3390/ijms22094599>
2. T. Shan, J. Ye, J. Jia, Z. Wang, Y. Jiang, Y. Wang, Y. Wang, K. Zheng, and Z. Ren, Viral UL8 is involved in the antiviral activity of oleanolic acid against HSV-1 infection, *Front. Microbiol.* **12** (2021) Article ID 689607 (12 pages); <https://doi.org/10.3389/fmicb.2021.689607>
3. N. Gupta, A review on recent developments in the anticancer potential of oleanolic acid and its analogs (2017-2020), *Mini Rev. Med. Chem.* **22**(4) (2022) 600–616; <https://doi.org/10.2174/1389557521666210810153627>
4. Y. Han, C. Wang, X. Li and G. Liang, Oleanolic acid reduces oxidative stress and neuronal apoptosis after experimental subarachnoid hemorrhage by regulating Nrf2/HO-1 pathway, *Drug Dev. Res.* **83**(3) (2022) 680–687; <https://doi.org/10.1002/ddr.21899>
5. E. Saberian, A. Jenča, A. Petrášová, J. Jenčová, R. A. Jahromi and R. Seiffadini, Oral cancer at a Glance, *Asian Pac. J. Cancer Biol.* **8**(4) (2023) 379–386; <https://doi.org/10.31557/apjcb.2023.8.4.379-386>
6. D. Jagadeesan, K. V. Sathasivam, N. K. Fuloria, V. Balakrishnan, G. H. Khor, M. Ravichandran, M. Solyappan, S. Fuloria, G. Gupta and G. Yadav, Comprehensive insights into oral squamous cell

- carcinoma: Diagnosis, pathogenesis, and therapeutic advances, *Pathol. Res. Pract.* **261** (2024) Article ID 155489; <https://doi.org/10.1016/j.prp.2024.155489>
7. A. Capote-Moreno, P. Brabyn, M. F. Muñoz-Guerra, J. Sastre-Pérez, V. Escorial-Hernandez, F. J. Rodríguez-Campo, T. García and L. Naval-Gías, Oral squamous cell carcinoma: epidemiological study and risk factor assessment based on a 39-year series, *Int. J. Oral Maxillofac. Surg.* **49**(12) (2020) 1525–1534; <https://doi.org/10.1016/j.ijom.2020.03.009>
  8. D. Vemula, P. Jayasurya, V. Sushmitha, Y. N. Kumar and V. Bhandari, CADD, AI and ML in drug discovery: A comprehensive review, *Eur. J. Pharm. Sci.* **181** (2023) Article ID 106324 (23 pages); <https://doi.org/10.1016/j.ejps.2022.106324>
  9. M. T. Muhammed and E. Aki-Yalcin, Molecular docking: principles, advances, and its applications in drug discovery, *Letf. Drug Des. Discov.* **21**(3) (2024) 480–495; <https://doi.org/10.2174/1570180819666220922103109>
  10. L. Zhao, H. Zhang, N. Li, J. Chen, H. Xu, Y. Wang and Q. Liang, Network pharmacology, a promising approach to reveal the pharmacology mechanism of Chinese medicine formula, *J. Ethnopharmacol.* **309** (2023) Article ID 116306; <https://doi.org/10.1016/j.jep.2023.116306>
  11. P. H. Patel, A. Jha and G. S. Chakraborty, *Role of Bioinformatics in Drug Design and Discovery*, in *CADD and Informatics in Drug Discovery* (Part of the book series: *Interdisciplinary Biotechnological Advances* (IBA)), Springer Nature Singapore, Singapore 2023, pp. 1–33.
  12. A. Daina, O. Michielin and V. Zoete, SwissADME: a free web tool to evaluate pharmacokinetics, drug-likeness and medicinal chemistry friendliness of small molecules, *Sci. Rep.* **7**(1) (2017) Article ID 42717 (13 pages); <https://doi.org/10.1038/srep42717>
  13. M. Gupta, H. J. Lee, C. J. Barden and D. F. Weaver, The blood–brain barrier (BBB) score, *J. Med. Chem.* **62**(21) (2019) 9824–9836; <https://doi.org/10.1021/acs.jmedchem.9b01220>
  14. A. Daina, O. Michielin and V. Zoete, SwissTargetPrediction: updated data and new features for efficient prediction of protein targets of small molecules, *Nucleic Acids Res.* **47**(W1) (2019) W357–W364; <https://doi.org/10.1093/nar/gkz382>
  15. Y. Liu, X. Yang, J. Gan, S. Chen, Z. X. Xiao and Y. Cao, CB-Dock2: Improved protein-ligand blind docking by integrating cavity detection, docking, and homologous template fitting, *Nucleic Acids Res.* **50**(W1) (2022) W159–W164; <https://doi.org/10.1093/nar/gkac394>
  16. C. M. McBride, B. Levine, Y. Xia, C. Bellamacina, T. Machajewski, Z. Gao, P. Renhowe, W. Antonios-McCrea, P. Barsanti, K. Brinner and A. Costales, Design, structure-activity relationship, and in vivo characterization of the development candidate NVP-HSP990, *J. Med. Chem.* **57**(21) (2014) 9124–9129; <https://doi.org/10.1021/jm501107q>
  17. T. Hu, J. E. Yeh, L. Pinello, J. Jacob, S. Chakravarthy, G. C. Yuan, R. Chopra and D. A. Frank, Impact of the N-terminal domain of STAT3 in STAT3-dependent transcriptional activity, *Mol. Cell. Biol.* **35**(19) (2015) 3284–3300; <https://doi.org/10.1128/MCB.00060-15>
  18. G. Q. Gong, B. Bilanges, B. Allsop, G. R. Masson, V. Robertson, T. Askwith, S. Oxenford, R. R. Madsen, S. E. Conduit, D. Bellini and M. Fitzek, A small-molecule PI3K $\alpha$  activator for cardioprotection and neuroregeneration, *Nature* **618**(7963) (2023) 159–168; <https://doi.org/10.1038/s41586-023-05972-2>
  19. J. R. López-Blanco, J. I. Aliaga, E. S. Quintana-Ortí and P. Chacón, iMODS: internal coordinates normal mode analysis server, *Nucleic Acids Res.* **42**(W1) (2014) W271–W276; <https://doi.org/10.1093/nar/gku339>
  20. A. Kuriata, A. M. Gierut, T. Oleniecki, M. P. Ciemny, A. Kolinski, M. Kurcinski and S. Kmiecik, CABS-flex 2.0: A web server for fast simulations of flexibility of protein structures, *Nucleic Acids Res.* **46**(W1) (2018) W338–W343; <https://doi.org/10.1093/nar/gky356>
  21. A. Maharati and M. Moghbeli, PI3K/AKT signaling pathway as a critical regulator of epithelial-mesenchymal transition in colorectal tumor cells, *Cell Commun. Signal.* **21**(1) (2023) Article ID 201 (15 pages); <https://doi.org/10.1186/s12964-023-01225-x>

22. Y. Cheng, J. Chen, Y. Shi, X. Fang and Z. Tang, MAPK signaling pathway in oral squamous cell carcinoma: biological function and targeted therapy, *Cancers* 14(19) (2022) Article ID 4625; <https://doi.org/10.3390/cancers14194625>
23. D. B. Doroshow, S. Bhalla, M. B. Beasley, L. M. Sholl, K. M. Kerr, S. Gnjatic, I. I. Wistuba, D. L. Rimm, M. S. Tsao and F. R. Hirsch, PD-L1 as a biomarker of response to immune-checkpoint inhibitors, *Nat. Rev. Clin. Oncol.* 18(6) (2021) 345–362; <https://doi.org/10.1038/s41571-021-00473-5>
24. M. E. Youssef, S. Cavalu, A. M. Hasan, G. Yahya, M. A. Abd-Eldayem and S. A. Saber, Role of ganetespib, an HSP90 inhibitor, in cancer therapy: from molecular mechanisms to clinical practice, *Int. J. Mol. Sci.* 24(5) (2023) Article ID 5014; <https://doi.org/10.3390/ijms24055014>
25. M. Niu, B. Zhang, L. Li, Z. Su, W. Pu, C. Zhao, L. Wei, P. Lian, R. Lu, R. Wang and J. Wazir, Q. Gao, S. Song and H. Wang, Targeting HSP90 inhibits proliferation and induces apoptosis through AKT1/ERK pathway in lung cancer, *Front. Pharmacol.* 12 (2022) Article ID 724192 (13 pages); <https://doi.org/10.3389/fphar.2021.724192>
26. H. A. Amisah, S. E. Combs and M. Shevtsov, Tumor dormancy and reactivation: the role of heat shock proteins, *Cells* 13(13) (2024) Article ID 1087; <https://doi.org/10.3390/cells13131087>
27. A. Bahmei, F. Karimi, S. M. Mahini, H. Irandoost, P. Tandel, H. Niknam and G. Tamaddon, Targeting telomerase with MST-312 leads to downregulation of CCND1, MDM2, MYC, and HSP90AA1 and induce apoptosis in Jurkat cell line, *Med. Oncol.* 41(11) (2024) Article ID 267; <https://doi.org/10.1007/s12032-024-02412-7>
28. M. Tolomeo and A. Cascio, The multifaceted role of STAT3 in cancer and its implication for anticancer therapy, *Int. J. Mol. Sci.* 22(2) (2021) Article ID 603; <https://doi.org/10.3390/ijms22020603>
29. Y. Hu, Z. Dong and K. Liu, Unraveling the complexity of STAT3 in cancer: Molecular understanding and drug discovery, *J. Exp. Clin. Cancer Res.* 43(1) (2024) Article ID 23 (29 pages); <https://doi.org/10.1186/s13046-024-02949-5>
30. S. Zou, Q. Tong, B. Liu, W. Huang, Y. Tian and X. Fu, Targeting STAT3 in cancer immunotherapy, *Mol. Cancer* 19 (2020) Article ID 145 (19 pages); <https://doi.org/10.1186/s12943-020-01258-7>
31. A. Jha, M. Alam, T. Kashyap, N. Nath, A. Kumari, K. K. Pramanik, S. Nagini and R. Mishra, Crosstalk between PD-L1 and Jak2-Stat3/MAPK-AP1 signaling promotes oral cancer progression, invasion, and therapy resistance, *Int. Immunopharmacol.* 124(Part A) (2023) Article ID 110894; <https://doi.org/10.1016/j.intimp.2023.110894>
32. S. Sharma and P. Kumar, Dissecting the functional significance of HSP90AB1 and other heat shock proteins in countering glioblastomas and ependymomas using omics analysis and drug prediction using virtual screening, *Neuropeptides* 102 (2023) Article ID 102383; <https://doi.org/10.1016/j.npep.2023.102383>
33. Y. J. Zhang and D. H. Yi, CDK1-SRC Interaction-dependent transcriptional activation of HSP90AB1 promotes antitumor immunity in hepatocellular carcinoma, *J. Proteome Res.* 22(12) (2023) 3714–3729; <https://doi.org/10.1021/acs.jproteome.3c00379>
34. X. Sun, K. Li, M. Hase, R. Zha, Y. Feng, B.-Y. Li and H. Yokota, Suppression of breast cancer-associated bone loss with osteoblast proteomes via Hsp90ab1/moesin-mediated inhibition of TGFβ/FN1/CD44 signaling, *Theranostics* 12(2) (2022) 929–943; <https://doi.org/10.7150/thno.66148>
35. P. Castel, E. Toska, J. A. Engelman and M. Scaltriti, The present and future of PI3K inhibitors for cancer therapy, *Nat. Cancer* 2(6) (2021) 587–597; <https://doi.org/10.1038/s43018-021-00218-4>
36. M. Zhang, H. Jang and R. Nussinov, PI3K inhibitors: review and new strategies, *Chem. Sci.* 11(23) (2020) 5855–5865; <https://doi.org/10.1039/d0sc01676d>